AD-A076 117 INSTITUTE FOR ACOUSTICAL RESEARCH MIAMI FLA F/G 20/1
EFFECTS OF OCEAN FRONTS ON MULTIPATH VERTICAL ANGLES AND THE AS--ETC(U)
JUL 79 R P FLANAGAN , X ZABALGOGEAZCOA N00014-74-C-0229
UNCLASSIFIED IAR-79002 NL

1 OF 1
AD-
A076117

END
DATE
FILMED
11-79
DDC

INSTITUTE FOR ACOUSTICAL RESEARCH
MIAMI DIVISION PALISADES GEOPHYSICAL INSTITUTE

EFFECTS OF OCEAN FRONTS ON MULTIPATH VERTICAL ANGLES AND THE ASSOCIATED BIASES IN ARRAY BEARING ESTIMATION*

R.P. Flanagan and X. Zabalgogeazcoa

Institute for Acoustical Research
615 Southwest Second Avenue
Miami, Florida 33130

July 1979

IAR 79002

Miami, Florida 33130

EFFECTS OF OCEAN FRONTS ON MULTIPATH VERTICAL ANGLES AND THE ASSOCIATED BIASES IN ARRAY BEARING ESTIMATION*

R.P. Flanagan and X. Zabalgogeazcoa

Institute for Acoustical Research
615 Southwest Second Avenue
Miami, Florida 33130

July 1979

IAR 79002

ABSTRACT

EFFECTS OF OCEAN FRONTS ON MULTIPATH VERTICAL ANGLES AND THE ASSOCIATED BIASES IN ARRAY BEARING ESTIMATION

R.P. Flanagan and X. Zabalgogeazcoa

An oceanic frontal system perpendicular to the propagation path is modeled with a deep receiver in warm water and a shallow source which is moved through the frontal system into progressively colder water. A ray model is used to calculate the arrival structure and determine the effects of the frontal system on ray amplitude and vertical angle. The receiving horizontal line array determines the bias in bearing estimation resulting from the changing multipath structure. This bias is found to be heavily dependent on array orientation and range into the frontal system while being only slightly dependent on array beamwidth. The underlying physics causing the multipath variations is the frontal system acting as a focusing lens. When the transducer positions are reversed, that is a deep receiver in cold water and a shallow source in progressively warmer water, the frontal system acts as a diverging lens.

Introduction

The propagation of sound through oceanic fronts is a topic of interest due to the frequent appearance of these systems in the world oceans. Typically an ocean front may be visualized as a well defined transition region between two volumes of water with characteristic sound velocity distributions. One of the effects of such a region in a propagation path is the alteration of the multipath structure of the received signal; in fact an oceanic front may act as an acoustic lens with either convergent or dispersive characteristics depending on the direction of transmission. Since source bearing estimation with a linear array is highly dependent on the vertical structure of the acoustic paths at the sensors one of the major effects of an oceanic front is the introduction of biased bearing estimation. The object of this paper is the determination of the magnitude of this bias for a typical frontal system anomaly.

In this study ray tracing techniques applied to an ocean with vertical and horizontal variations in the sound velocity profile have been used to analyze the effect of a frontal system on acoustic transmission. The bulk of the material is concerned with a source located in progressively colder water propagating a 200 Hz CW signal through the frontal system to a warm water array. After the multipath structure, arrival angle, bearing estimation and bias are thoroughly presented for this transducer geometry the positions of the source and receiver are

reversed and a brief examination of the frontal effects is made. In both cases the bias in bearing estimation introduced by the frontal system was found to be a function of range, beamwidth, and directional orientation of the array.

I. The Frontal System

An oceanic front may be defined as the transition region which divides water masses of different physical characteristics with the surface positions of the fronts being marked by strong horizontal temperature gradients. These fronts tend to remain in one area, but can exhibit severe variations within that area.[1-2] A general outline of the frontal systems of the world oceans along with their seasonal positions is given by Laevastu and LaFond.[3] Work on specific systems includes Levenson and Doblar[4] for the North Atlantic, Roden[5] for the North Pacific and Bannister, et. al.[6] for the South Tasman Sea.

The system we have chosen to model is bi-frontal and extends from warm to cold water regions, (Fig. 1). Proceeding from warm to cold water the first region has a profile with a negative gradient extending from the surface to the SOFAR axis. The profile for the second region has a near isovelocity layer extending from the surface to 150 m. Beyond that depth the sound velocities gradually merge to form an elevated SOFAR axis. The area separating these two regions is termed the first front and is 50 km wide. The third region contains the coldest water and has a near isovelocity layer in the upper 200 m joined to a positive gradient below that depth. The second front, which separates regions 2 and 3, is also 50 km wide. Because of the imaginary location of the receiving array, and thus its variability in range, it is possible to examine the propagation of sound for both the single and double front cases.

The top half of Fig. 1 shows the location of the fronts with range. The receiver is at 2100 m in the warm water profile while the 100 m deep source was placed at ranges varying from 700 to 1125 km. Each region has a range independent sound velocity while the fronts contain the transition profiles between surrounding regions.

The fronts are taken to be perpendicular to the propagation path. If this is not the case horizontal refraction takes place and the rays propagate out of the vertical plane indicating a source of bearing bias which will not be examined here. Finally, the width of the front will affect the bias in bearing estimation. Calculations with a front width of 5 km showed rapid oscillations of this bias with range. This occurs because the rays alternately sample and miss the front since the anomaly decreases in amplitude with depth and the rays may therefore pass under it at certain ranges.

II. The Ray Model

The ray model used for this study is described elsewhere[7] and is capable of tracing rays in a medium with vertical and horizontal variations in the sound speed profile. The basic profile consisted of four pieces with a linear bottom section, two hyperbolic cosines for the SOFAR region, and a surface section with a sound velocity distribution that yields a conic ray path. The horizontal variation of the profiles occurred only in the two frontal regions with range steps of 100 m. The bottom was assumed to be flat and lossy to limit the significant arrivals to refracted-refracted (RR) and refracted-surface reflected (RSR) rays. The corresponding profiles and profile anomalies are shown in the lower half of Fig. 1 and Fig. 2 respectively. It can be seen that the anomalies for these two fronts are similar in general form.

III. The Array Reception Model

The receiving array was modeled as a horizontal linear set of phones. In order to avoid specifying the number, separation distances, and shading of the phones, the calculations were performed for 3 dB beamwidths of 1^{o}, 2^{o} and 5^{o} with sin x/x weightings. The range of beamwidths was based on the examination of several papers on arrays a few of which are ref. 8-11. Typically beamwidth broadens when passing from broadside to endfire aspects so the results for the different beamwidths can be mixed to more accurately depict this. The array reception as a function of array axis orientation with respect to the frontal system was simulated. The array axis was rotated from a position parallel to the fronts to the perpendicular position in 1^{o} increments. For each array orientation the array response as a function of azimuth (θ) was obtained by means of the incoherent beamformer.

$$P(\theta) = \int_{0}^{L} \sum_{n=1}^{N} A_n \exp\left\{ j \left[\underset{\sim}{k}_n(\theta_s, \mu_n) - \underset{\sim}{k}_o(\theta) \right] \cdot \underset{\sim}{x} \right\} dx$$

where A_n and $\underset{\sim}{k}_n$ are the amplitudes and vector wave numbers of the N paths determined by the ray tracing model, μ_n is the vertical elevation of the paths, $\underset{\sim}{k}_o$ is the horizontal array steering vector and L is a parameter that adjusts the desired beamwidth.

The geometry of the array is shown in Fig. 3. The main lobe corresponding to a steering to azimuth θ_o is

shown as a figure of revolution about the array axis. If a source is located at azimuth θ_s only rays reaching the array with vertical arrival angles between μ_{MIN} and μ_{MAX} will be processed in the beamformer output.

Figures 4 and 5 show vertical angle of arrival vs bearing (0^o being endfire) for 1^o and 5^o beamwidths. From these plots it is possible to obtain a bearing estimate. The two horizontal lines on Fig. 5 indicate arrivals with vertical angles of 7.5^o and 15^o. Let the vertical line at 20^o bearing represent the true bearing of the source. The intersection of these lines at points A and B may be continued to the bearing axis by the dashed lines. Apparent bearings of 21.25^o and 25^o yield biases of 1.2^o and 5^o for the two rays. If equi-amplitude rays are chosen then an averaging process can be used to set the bias at 3.1^o. If the true bearing is 50^o the points C and D convert to biases of $.3^o$ and 1.8^o with an average of 1.0^o. From the comparison of these two examples it can be seen that this bias is a function of array orientation with the largest biases occurring in the endfire aspect.

If ray amplitudes are different another method of determining the bias in bearing estimate is needed. These characteristics necessitated the incoherent summation of the rays over a specified beamwidth and weighting function described previously. A three dimensional plot of array energy vs true bearing from

array vs apparent bearing from array yields a visual representation of the bias in bearing estimation as will be shown for the specific front process.

IV. The Computer Simulation

The ray model was run at various ranges before the fronts and in the fronts. The ranges within the frontal region were also run without the frontal effects in order to examine the changes that the fronts had caused. All of the data was examined with beamwidths of 1^{o}, 2^{o} and 5^{o}.

As an example, three dimensional plots and the resultant bearing bias vs true bearing diagrams are given for ranges of 875 and 910 km and a 1^{o} beamwidth. Figure 1 shows these two ranges to be in the center of and 10 km after the first front respectively. Figures 6 and 7 represent the array response for these ranges without the fronts, and Figs. 8 and 9 depict the complementary data but include the frontal effects. Figure 10 depicts the bias in bearing for each of the four cases above. Examining Fig. 6 with a bearing of source from array of 0^{o}, three peaks are observed at apparent bearings of 9.5^{o}, 11.1^{o}, and 13.6^{o}. These peaks represent the energy from ray pairs, each pair with the same number of cycles between the source and receiver and consisting of a positive and negative angle at the source. It is apparent that a horizontal array in the endfire aspect, with a beamwidth and directional increment of $.1^{o}$ can separate ray arrivals with vertical angle differences of twice the beamwidth if the array operates as presumed. As the array is moved towards broadside the ability to separate ray arrivals is lost. This is observable from

Fig. 4 as the range of vertical angle increases for constant bearing as bearing is increased. Returning to Fig. 6 we define the apparent bearing (bearing estimate) of the source from the array as the point of maximum energy; then 11.1° is the bearing bias. Naturally it is desirable to make the bias as small as possible and we would like to pick the peak at 9.5°. This could be acomplished if we used the first deviation from zero as apparent bearing is increased, however it may not be possible to determine if it is single or multiple sources creating the multi-bearing readings.

Comparing Fig. 6 with 8 and Fig. 7 with 9 we can examine the effects of the first front. There appears to be more energy for the frontal cases, and it is shifted towards the lower end of the apparent bearing axis reducing the bearing bias. This is also indicated in Fig. 10. Figures 11 and 12 show the amplitudes of the positive source angle rays which reach the array with vertical angle θ_R for the cases without the front and with the front respectively. The arrival sets are shown for different ranges and the location of these points with respect to the frontal regions can be determined from Fig. 1. Examining the two Figs. at 875 km and 910 km there is a definite increase in the number of arrivals and a decrease in θ_R for the arrivals when the effects of the frontal region are included.

One simple case is presented in the Appendix showing transmission from cold to warm water through a front focuses the multipath structure. That is, rays from the cold water which interacted with the surface will not reach the surface in warmer waters. Therefore, the acoustics with the cold to warm water front and these approximate source and receiver depths should support more RR type rays with higher cycle number and lower θ_R than the acoustics without the front.

Figure 13 depicts the arrival pattern for the positive source angles before the fronts from 750 km to 850 km. It is possible to detect trends in this pattern. If the bases of the rays are joined in the 760 km to 810 km ranges a shape is formed similar to the greek letter μ with the final tail clipped off. Figure 14 is an expansion of the previous figure including ranges from 750 km to 1100 km without the frontal process. Each μ shape here represents rays with the same cycle number as indicated on the figure. Because there are no horizontal variations, i.e., profile 1 is used throughout, the angles may be found where propagation type changes from RR to RSR to SRBR. These divisions are indicated on the plot. A rough approximation of spreading loss can be determined by examining $dR/d\theta_R$ of each curve. Large values of this derivative indicate low amplitudes while small values indicate large amplitudes. Therefore, the amplitudes of the RR ray types increase as θ_R decreases. The RSR rays have low amplitudes at the transition regions and large amplitudes in the "valley"

regions indicated in the figure. Further, because $dR/d\theta_R$ is larger there, the RSR rays on the left side of the valley have lower amplitude than those on the right. The SRBR rays have consistently high losses due to spreading which are further magnified by the bottom losses, so these rays will not be mentioned any further. Using this figure it is possible to determine the number and type of ray solutions at a given range. For example, at 900 km the arrival set consists of a 16 cycle RR ray and two 16 cycle RSR rays. At 1040 km the arrival set contains one RR and two RSR rays with 18 cycles and the same types with 19 cycles.

The bias in bearing estimation can be examined using this figure and the general rule that an increase in vertical angle causes an increase in bearing bias. Starting at 750 km and increasing range the angle of the arrival with the largest amplitude at each range will indicate the bearing bias. From 750 km to 850 km at 10 km intervals the angles are: 8.8, 10.5, 8.2, 8.3, 8.5, 9.7, 8.8, 11.1, 8.3, 8.4, 8.6 degrees. The pattern here consits of a jump in angle followed by a smooth rise to the next jump followed by a smooth rise. This data is presented as a part of Fig. 15. The dashed lines mark the boundaries of the indicated cycle number. The constant slope is the RR region while the peak is formed by the RSR ray. From Fig. 14 it can be seen that the peak formed by the 13 cycle RR ray does not

continue into the valley formed by the 14 cycle RSR ray therefore, there is a large change in the vertical angle for the 13 cycle ray as shown in Fig. 15. Prior to 750 km this peak is presented in each ray cycle. As range is increased beyond 1100 km the peak formed by the N cycle RR ray reaches further into the valley of the N+1 cycle RR ray and ultimately the RR rays dominate the vertical angle and thus the bearing bias. At that range the plot similar to Fig. 15 should consist of only the small slopes. As the beam reaches broadside the bias in bearing estimation decreases rapidly.

Unfortunately, Figs. 14 and 15 are not as readily constructed for the cases including the fronts. The arrival pattern is available for only the specific ranges examined. The bias in bearing estimate is presented for 1° and 5° beamwidths in Tables 1, 2 and 3. Fig. 16 presents the bearing bias at endfire for the sampled ranges. From 750 km to 850 km a pattern similar to that in Fig. 15 is present but once the fronts are encountered the data is not sampled finely enough to discern a new pattern. However, it can be seen that the first front does decrease the bias as predicted by the focusing effect.

The multipath vertical angle pattern for the acoustics passing through both fronts is presented in the upper portion of Fig. 12. It can be seen that the number of arrivals has increased and there are several

rays with lower vertical angles at the receiver when compared to the multipath passing through the first front only. Figure 16 includes the bearing bias at endfire for ranges into the 2nd front. Although the decrease in bias is not as smooth as at the first front it does exist indicating a continuing focusing of the multipath structure.

We will now briefly examine the effects of the same frontal system on propagation between a shallow source in warm water and a deep receiver in cold water. The multipath structure as a function of range is shown in Fig. 17. A repeating pattern is present up to 1090 km indicating the passage of the source through the first front (front 2 in Figs. 1 and 16) has done little to affect the propagation. However, as the source passes through the second front (front 1 in Figs. 1 and 16) a significant change in the multipath structure takes place. The major arrival pair changes its vertical angle at the receiver from 3^{o} to 6^{o}. Thus the frontal system combined with this source and receiver orientation acts as a weak dispersive lens once the source is in the warm water. Figure 18 depicts the bias in the bearing estimate at the endfire aspect for receivers located in both warm and cold water. The different patterns in the bias for the two cases are present from 750 to 850 km. Beyond the second front the bias has decreased 5^{o} for the warm water receiver while it has increased 3^{o} for the cold water receiver.

V. Results and Conclusions

The effect of an ocean front on the multipath vertical angles and the associated bias in bearing estimation was found to be highly dependent of array orientation. At endfire the maximum bias was 11° while beyond 30° from endfire the bias was reduced to less than 2° for the various ranges and frontal conditions examined. The bias was found to exhibit a somewhat periodic pattern with range with the amplitudes of the variations decreasing with increasing range. Beamwidth was found to affect the bias in bearing estimate to a lesser degree and the apparent bearing of the source was always directed towards broadside.

It was also found that the frontal system acted as a convergent or dispersive lens depending on the direction of propagation. For a warm water receiver the frontal system decreased the bias in the bearing estimate at endfire by 5° while this bias was increased by 3° for a cold water receiver. It was further shown that a narrow beamwidth horizontal array should be able to separate individual multipath arrivals at endfire.

Acknowledgement

This work was supported by the Office of Naval Research, Code 222.

APPENDIX

Multipath sound propagation through a cold to warm water front, subcripted c and w respectively, will undergo a focusing effect when the ray passes under the anomaly.

Referring to Fig. A1, the ray travels from cold to warm water, passing under the anomaly of depth Z_A. Here Z_{V_w} and Z_{V_c} refer to the vertex depths near the surface. Because

$$C_c = C_w;\ \theta_c = \theta_w \text{ and } C_{V_c} = C_{V_w} \tag{A1}$$

it is apparent from the diagram that

$$Z_{V_w} > Z_{V_c}. \tag{A2}$$

1^{o} Beamwidth

	Bearing of Source from Array								
Range	0	6	12	18	24	30	36	42	48
850	8.6	4.5	2.8	1.9	1.5	1.1	.9	.8	.8
875	11.1	6.6	4.4	3.1	2.1	1.6	1.4	1.1	.9
910	8.7	4.7	2.8	2.0	1.5	1.1	1.0	.9	.8
1065	8.6	4.5	2.7	1.8	1.4	1.1	.9	.8	.8
1090	11.1	4.8	3.0	2.1	1.8	1.5	1.3	1.1	.9
1125	8.7	4.6	2.8	1.9	1.4	1.1	.9	.8	.7

5^{o} Beamwidth

	Bearing of Source from Array								
Range	0	6	12	18	24	30	36	42	48
850	9.3	5.5	3.7	2.7	2.1	1.6	1.3	1.1	.9
875	10.8	6.4	4.3	3.0	2.3	1.8	1.5	1.3	1.1
910	9.3	5.5	3.8	2.6	2.0	1.7	1.3	1.0	.9
1065	9.5	5.7	3.8	2.8	2.2	1.7	1.4	1.1	.9
1090	10.2	5.8	3.8	2.7	2.1	1.7	1.3	1.1	.9
1125	9.6	5.9	4.0	3.0	2.3	1.8	1.5	1.3	.9

Table 1 - Bearing Bias : No Fronts

1° Beamwidth

	Bearing of Source from Array								
Range	0	6	12	18	24	30	36	42	48
850	8.6	4.5	2.8	1.9	1.5	1.1	.9	.8	.8
875	6.2	2.8	1.7	1.2	.9	.7	.7	.6	.5
910	4.8	1.8	1.2	.8	.7	.5	.4	.3	.3
1065	5.3	2.0	.9	.5	.5	.4	.3	.3	.3
1090	3.1	.6	.4	.3	.3	.2	.2	.2	.1
1125	3.1	.8	.5	.4	.4	.4	.3	.3	.3

5° Beamwidth

	Bearing of Source from Array								
Range	0	6	12	18	24	30	36	42	48
850	9.3	5.5	3.7	2.7	2.1	1.6	1.3	1.1	.9
875	7.3	3.7	2.5	1.8	1.4	1.1	.9	.7	.6
910	5.9	2.2	1.6	1.3	1.0	.8	.7	.5	.5
1065	4.3	1.9	1.4	1.1	.9	.7	.6	.5	.4
1090	3.4	1.2	.8	.7	.6	.5	.4	.3	.3
1125	4.6	2.1	1.5	1.3	1.0	.8	.7	.6	.5

Table 2 - Bearing Bias : Fronts

1° Beamwidth

	Bearing of Source from Array								
Range	0	6	12	18	24	30	36	42	48
750	8.8	4.7	2.9	2.0	1.5	1.1	1.0	.8	.8
760	10.6	6.1	3.8	2.7	2.0	1.6	1.3	1.1	.8
770	8.2	4.2	2.5	1.8	1.3	1.1	.9	.7	.6
780	8.4	4.4	2.7	1.9	1.4	1.1	.9	.8	.7
790	8.6	4.5	2.8	1.9	1.4	1.1	.9	.8	.7
800	8.7	4.6	2.8	2.0	1.5	1.1	1.0	.8	.8
810	8.8	4.7	2.9	2.1	1.6	1.1	1.0	.8	.8
820	11.2	6.7	4.3	2.9	2.1	1.6	1.3	1.1	.9
830	8.4	4.3	2.6	1.8	1.4	1.1	.9	.8	.7
840	8.5	4.4	2.7	1.9	1.4	1.1	.9	.8	.8

5° Beamwidth

	Bearing of Source from Array								
Range	0	6	12	18	24	30	36	42	48
750	9.5	5.7	3.9	2.8	2.2	1.7	1.4	1.1	.9
760	10.5	6.1	4.0	2.8	2.2	1.7	1.4	1.1	.9
770	8.8	4.7	3.1	2.2	1.7	1.3	1.1	.9	.7
780	9.2	5.2	3.5	2.6	2.0	1.6	1.3	1.0	.9
790	9.3	5.3	3.5	2.5	1.9	1.5	1.2	1.0	.8
800	9.4	5.5	3.7	2.7	2.1	1.6	1.3	1.1	.9
810	9.5	5.6	3.8	2.8	2.2	1.7	1.3	1.1	.9
820	10.7	6.3	4.1	3.0	2.3	1.8	1.4	1.2	.9
830	9.1	5.1	3.4	2.5	1.9	2.3	1.2	1.0	.8
840	9.3	5.4	3.7	2.7	2.1	2.5	1.3	1.1	.9

Table 3 - Bearing Bias : Before Fronts

REFERENCES

* Part of this paper was presented at the 95th Meeting of the Acoustical Society of America, Providence, R.I.

1. R.W. James, Criticality of Ocean Fronts to ASW Operations, NAVOCEANO Technical Note 7700-3-72, 1 Sept. 1972.
2. G. Neumann and W. Pierson, Jr., Principles of Physical Oceanography, Prentice Hall, Inc. Englewood Cliffs, N.J., 1966.
3. T. Laevastu and E.C. LaFond, Oceanic Fronts and Their Seasonal Positions on the Surface, Naval Undersea Research and Development Center, Technical Publication NUC TP 204, October 1970.
4. C. Levenson and R.A. Doblar, "Long-range Acoustic Propagation through the Gulf Stream", J. Acoust. Soc. Am., 59, 1134-1141 (1976).
5. G.I. Roden, "Oceanic Subarctic Fronts of the Central Pacific: Structure of and Response to Atmospheric Forcing", J. Phys. Ocean., 7, 761-778 (1977).
6. R.W. Bannister, R.N. Denham, K.M. Guthrie, and D.G. Browning, "Project TASMAN TWO: Low-Frequency Propagation Measurements in the South Tasman Sea", J. Acoust. Soc. Am., 62, 847-859 (1977).
7. N.L. Weinberg and X. Zabalgogeazcoa, "Coherent Ray Propagation through a Gulf Stream Ring", J. Acoust. Soc. Am., 62, 888-894 (1977).

8. F.N. Spiess, B. Luyendyk, M.S. Loughridge, "Bottom Slope Distributions and Implied Acoustic Bearing Errors in Abyssal Hill Regions of the North Pacific", J. of Underwater Acoustics, 183-196 (1969) Unclassified.

9. T.W. Sjoding, "Some Beam-steering Properties of Discretely Phased Symmetric Arrays", J. Acoust. Soc. Am., 54, 1347-1351 (1973).

10. D.D. Baker, D.A. Smith, "Study of the Measurement of Transducer Directivity with a Planar Measurement Array", J. Acoust. Soc. Am., 58, 807-811 (1975).

11. C.M. McKinney, R.H. Wallace, "Underwater Sound Transducer Beam Control with Reflectors", J. Acoust. Soc. Am., 55, 1190-1196 (1974).

List of Figures

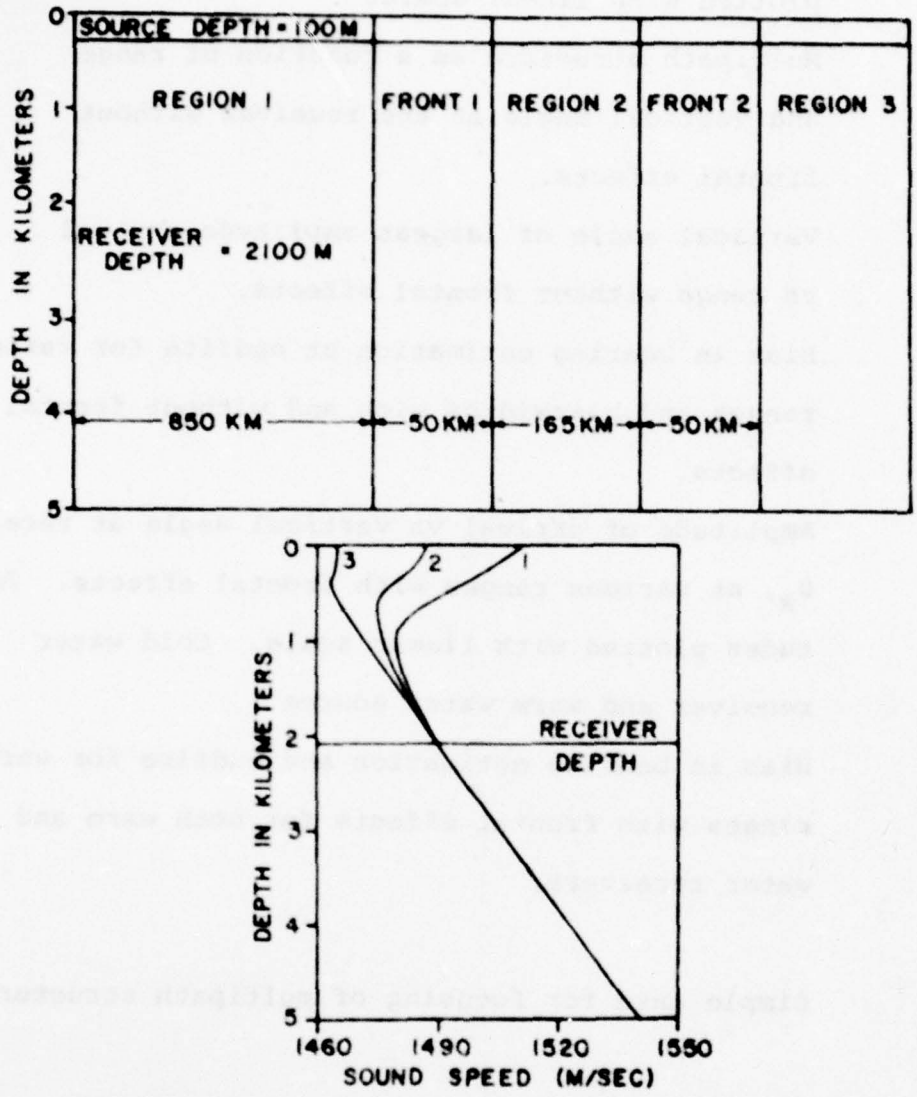

FRONTAL SYSTEM GEOMETRY AND SOUND SPEED PROFILES

FIG. 1

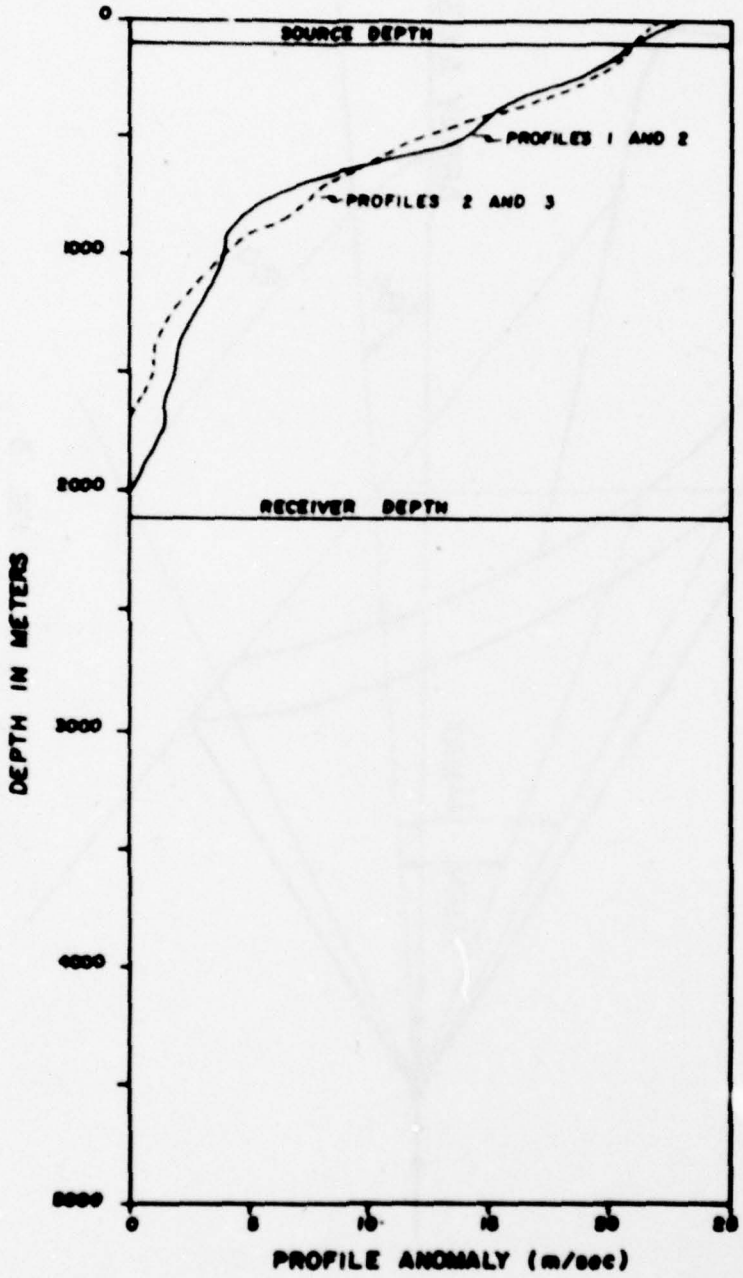
SOURCE DEPTH
PROFILES 1 AND 2
PROFILES 2 AND 3
RECEIVER DEPTH
DEPTH IN METERS
PROFILE ANOMALY (m/sec)

FIG. 2

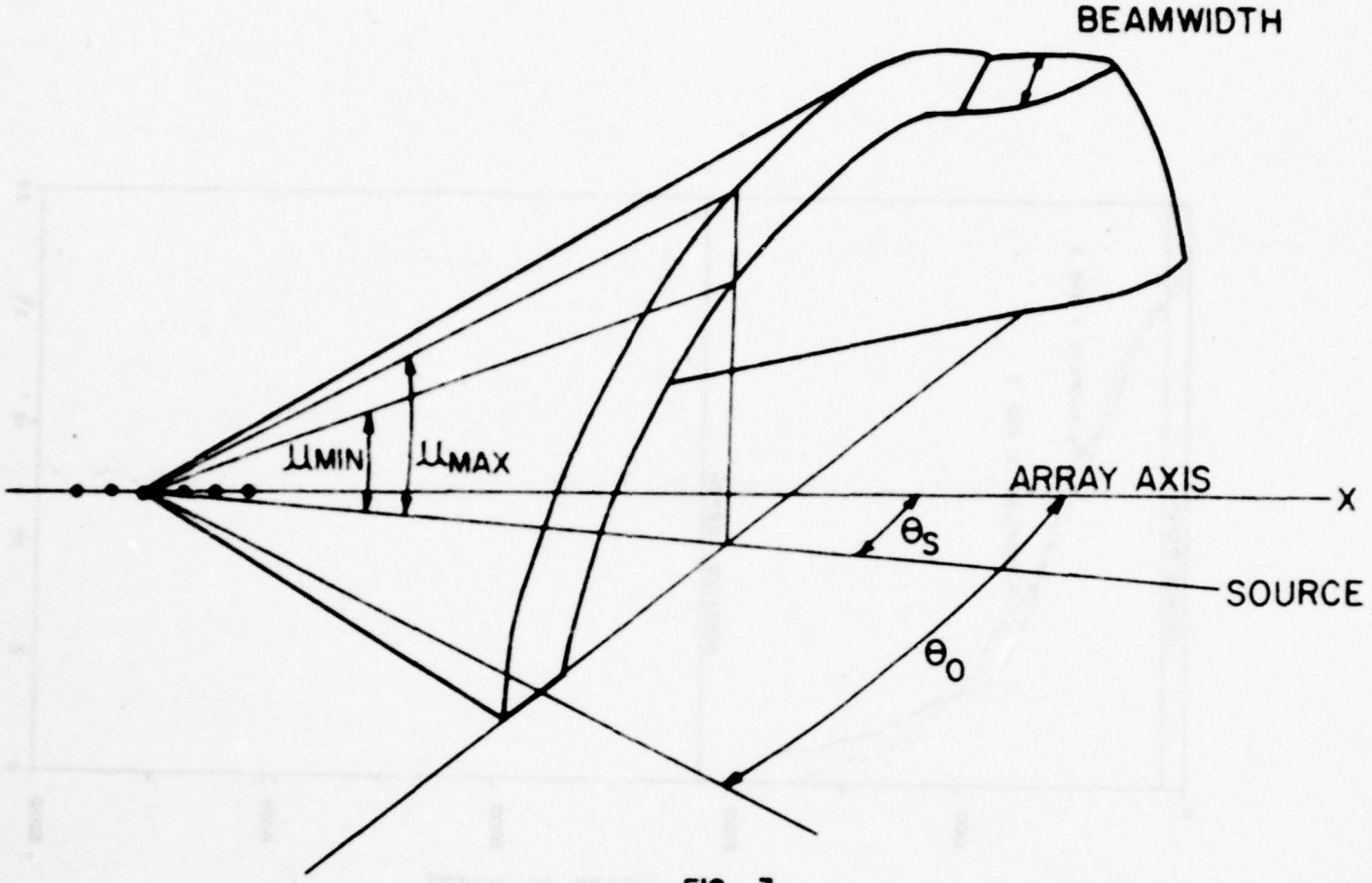

FIG. 3

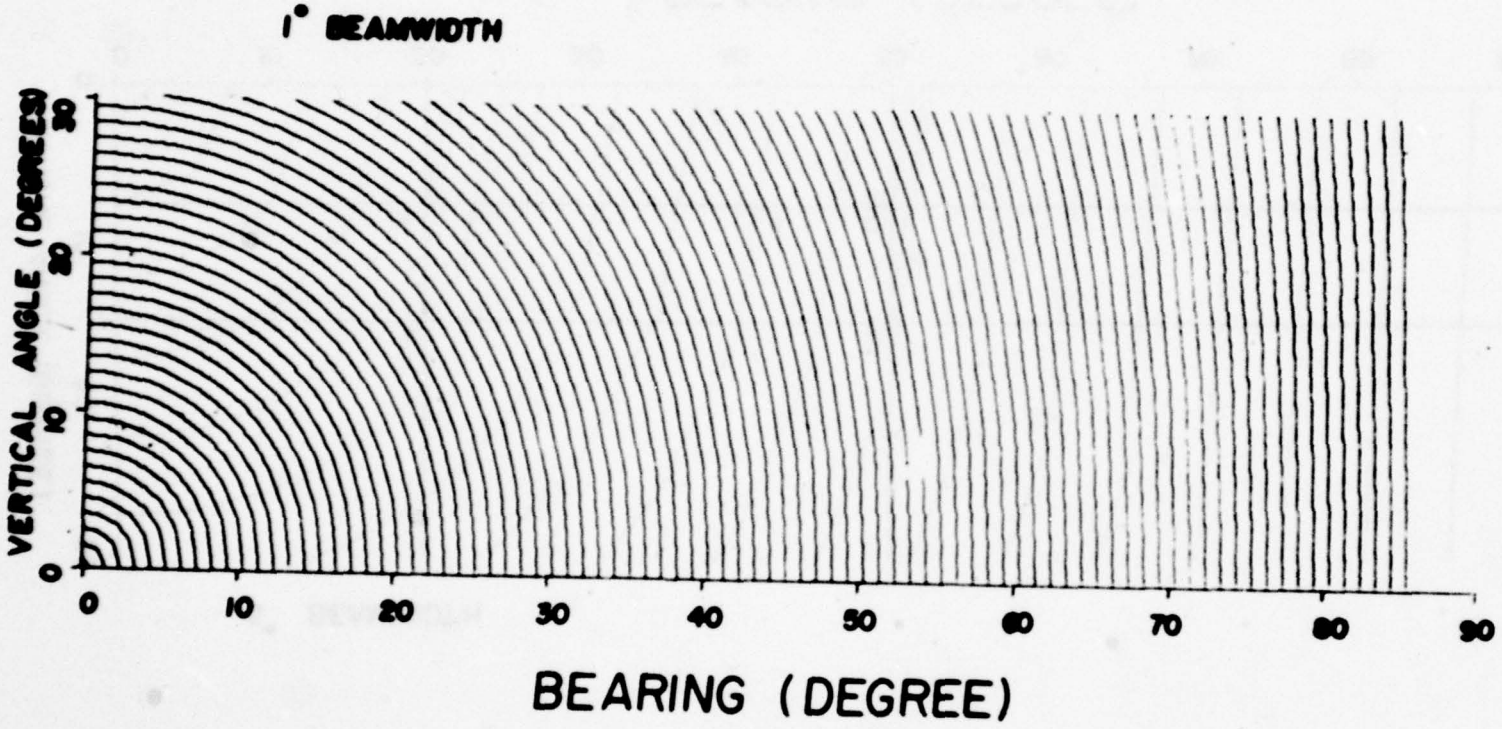
1° BEAMWIDTH
VERTICAL ANGLE (DEGREES)
0
10
20
30
0
10
20
30
40
50
60
70
80
90
BEARING (DEGREE)

FIG. 4

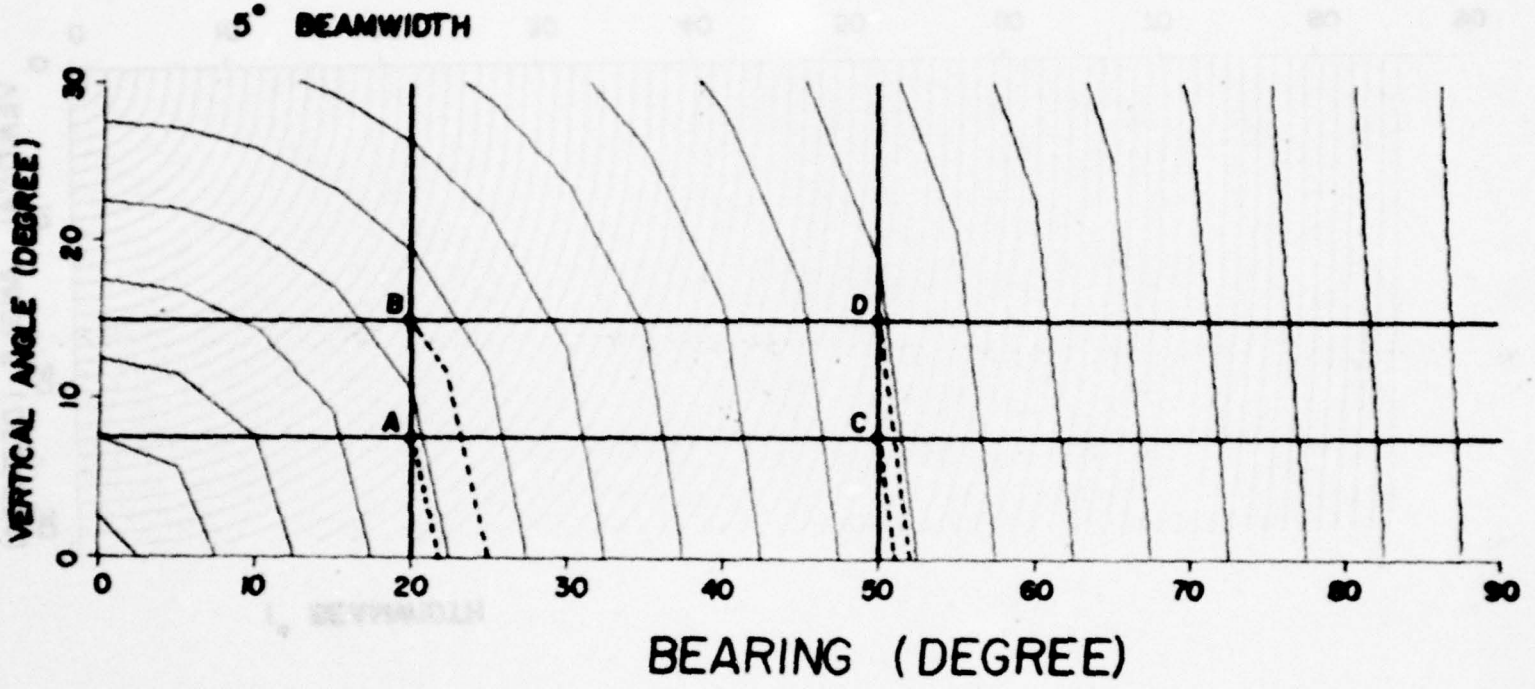
5° BEAMWIDTH
VERTICAL ANGLE (DEGREE)
0
10
20
30
A
B
C
D
0
10
20
30
40
50
60
70
80
90
BEARING (DEGREE)

FIG. 5

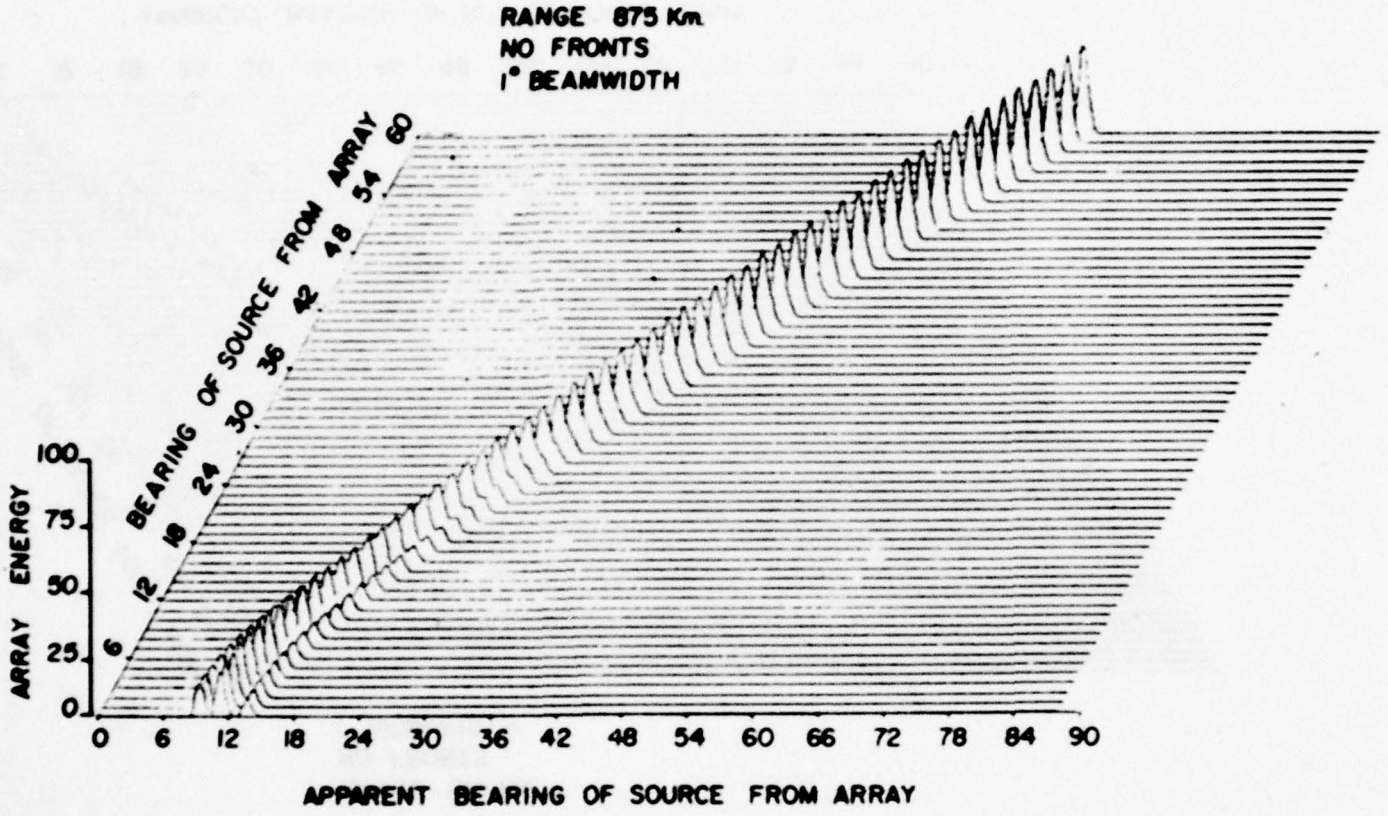
RANGE 875 Km
NO FRONTS
1° BEAMWIDTH
BEARING OF SOURCE FROM ARRAY
6
12
18
24
30
36
42
48
54
60
ARRAY ENERGY
100
75
50
25
0
0
6
12
18
24
30
36
42
48
54
60
66
72
78
84
90
APPARENT BEARING OF SOURCE FROM ARRAY

FIG. 6

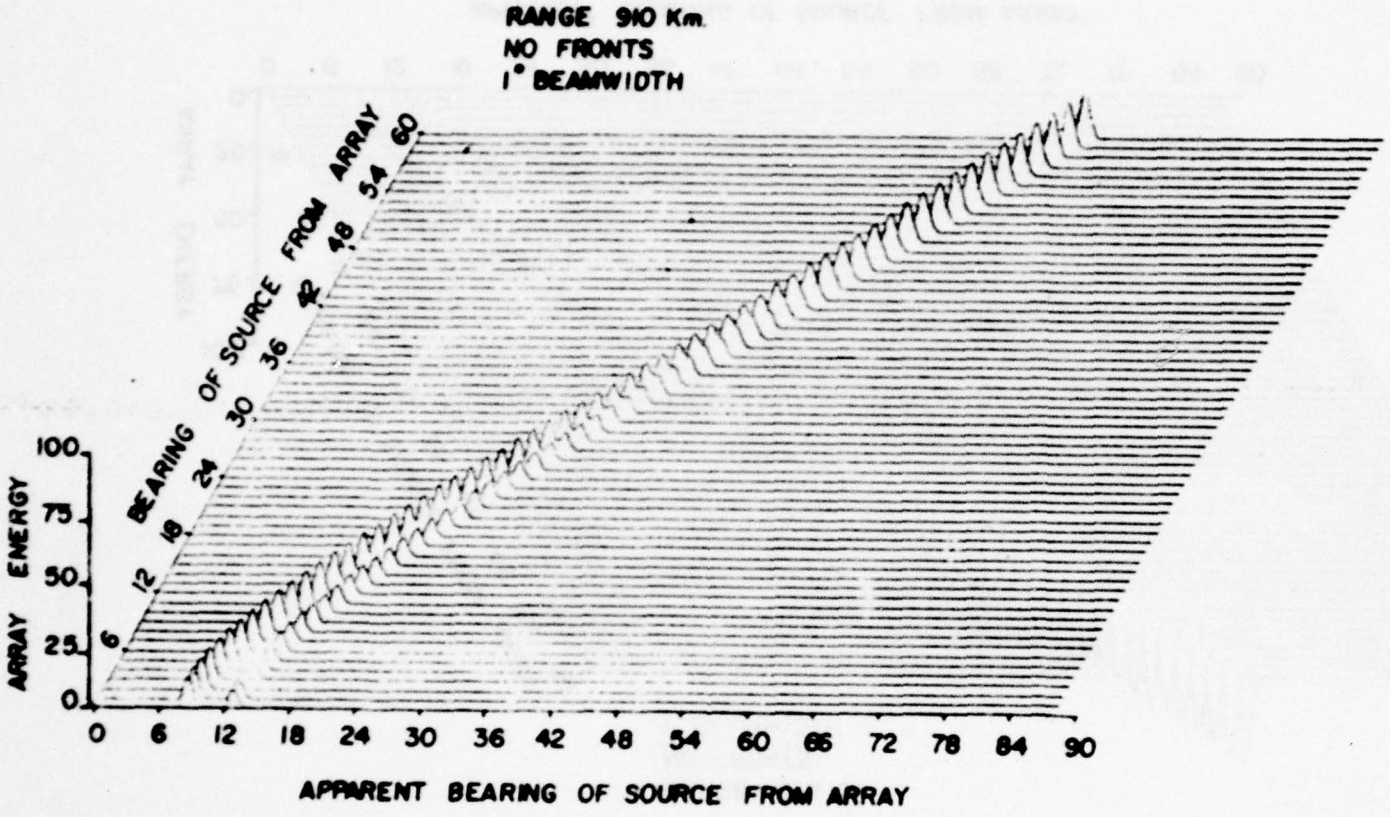
RANGE 910 Km.
NO FRONTS
1° BEAMWIDTH
BEARING OF SOURCE FROM ARRAY
6
12
18
24
30
36
42
48
54
60
ARRAY ENERGY
100
75
50
25
0
0
6
12
18
24
30
36
42
48
54
60
66
72
78
84
90
APPARENT BEARING OF SOURCE FROM ARRAY

FIG. 7

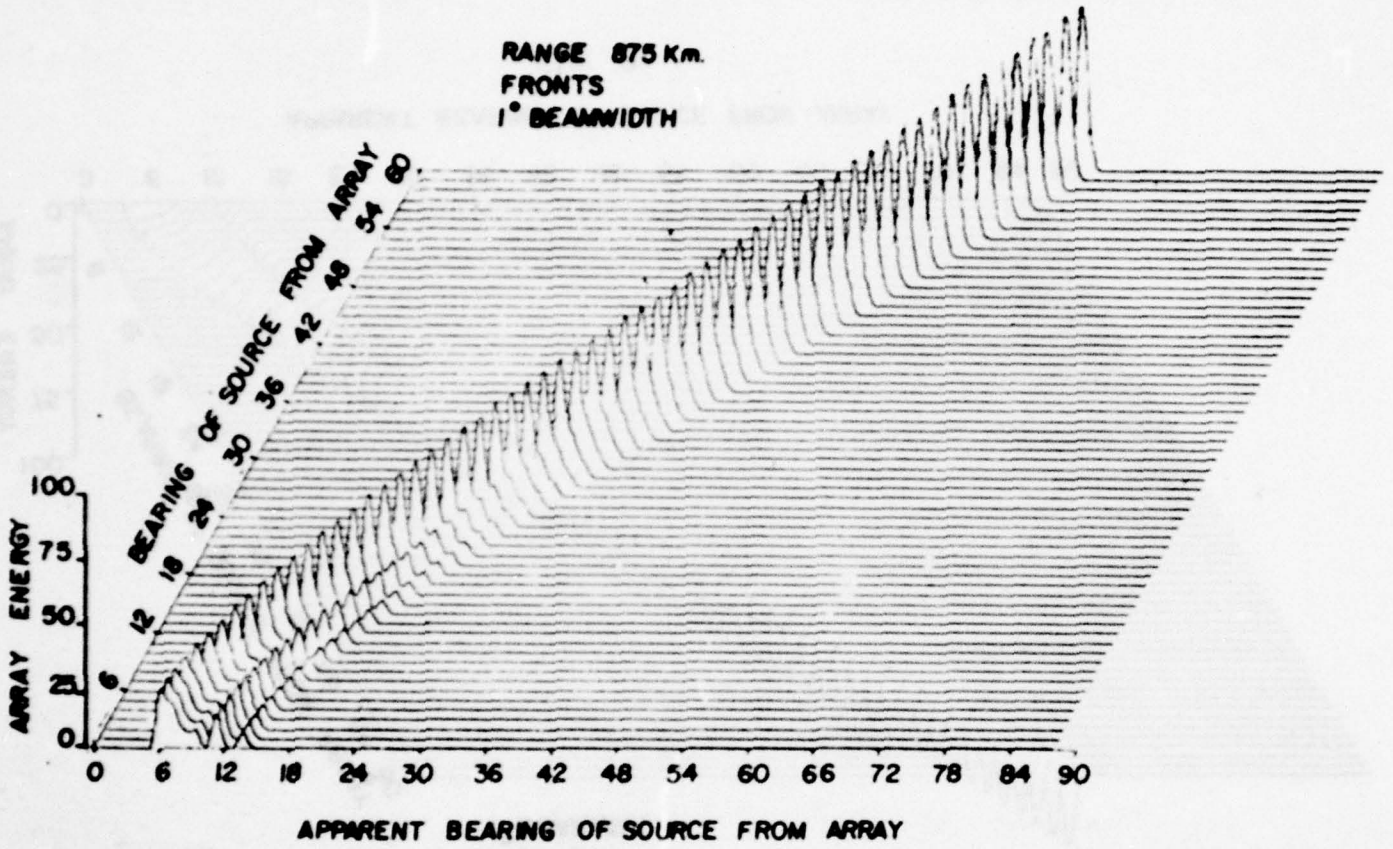
RANGE 875 Km.
FRONTS
1° BEAMWIDTH
BEARING OF SOURCE FROM ARRAY
6
12
18
24
30
36
42
48
54
60
ARRAY ENERGY
100
75
50
25
0
0
6
12
18
24
30
36
42
48
54
60
66
72
78
84
90
APPARENT BEARING OF SOURCE FROM ARRAY

FIG. 8

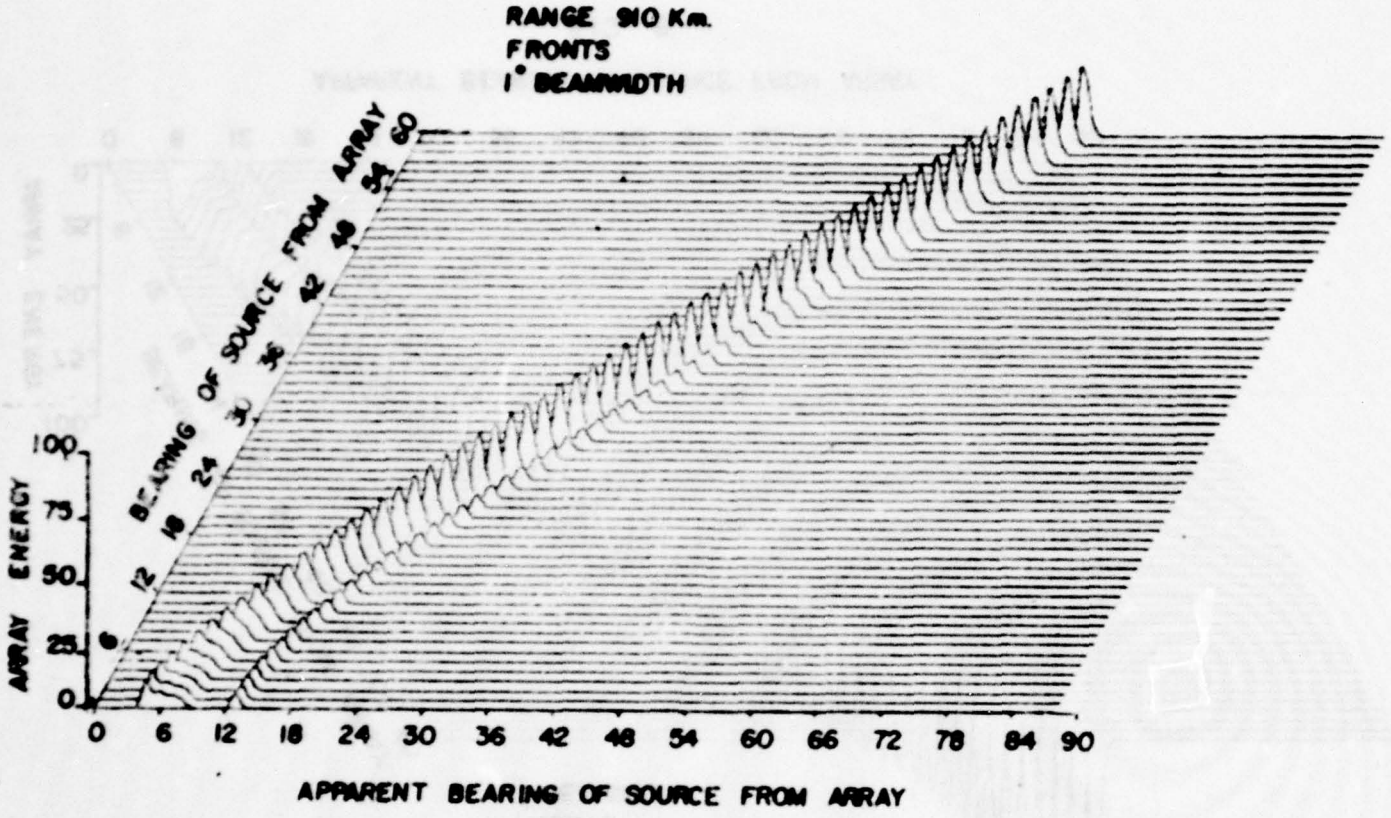
RANGE 910 Km.
FRONTS
1° BEAMWIDTH
BEARING OF SOURCE FROM ARRAY
0
6
12
18
24
30
36
42
48
54
60
ARRAY ENERGY
100
75
50
25
0
0 6 12 18 24 30 36 42 48 54 60 66 72 78 84 90
APPARENT BEARING OF SOURCE FROM ARRAY

FIG. 9

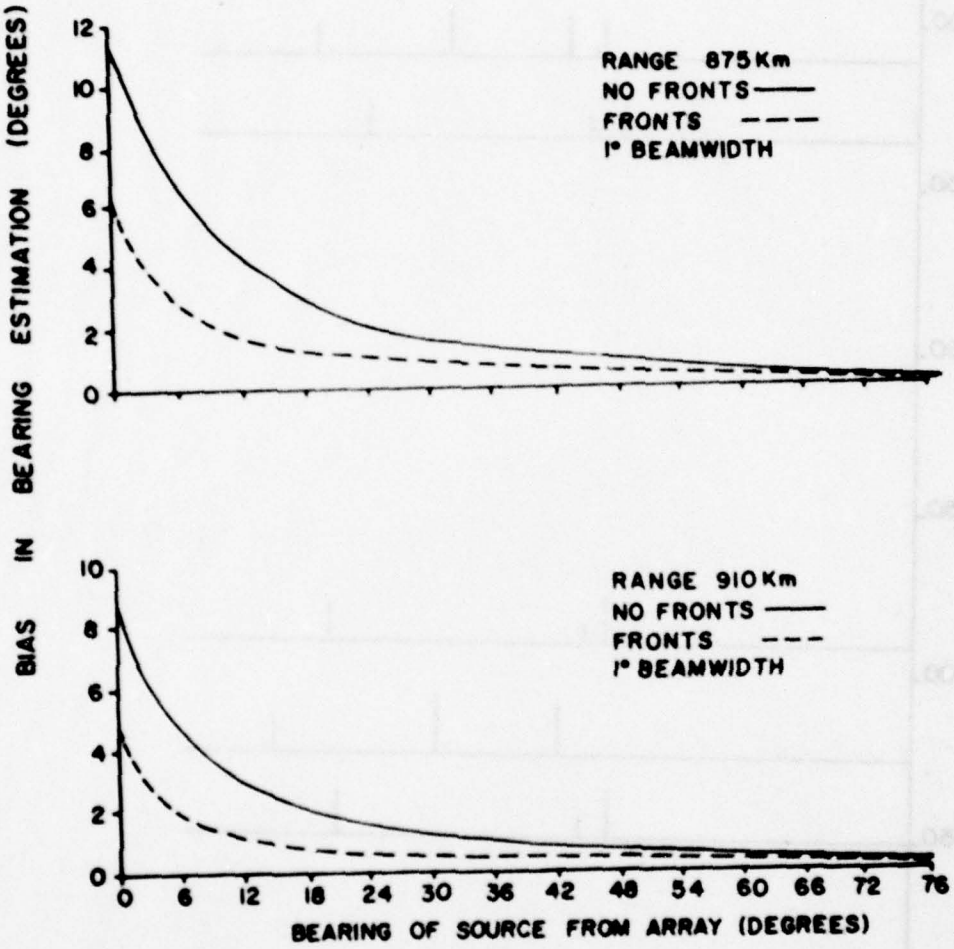
BIAS IN BEARING ESTIMATION (DEGREES)
RANGE 875Km
NO FRONTS
FRONTS
1° BEAMWIDTH
RANGE 910Km
NO FRONTS
FRONTS
1° BEAMWIDTH
0
2
4
6
8
10
12
0 6 12 18 24 30 36 42 48 54 60 66 72 76
BEARING OF SOURCE FROM ARRAY (DEGREES)

FIG. 10

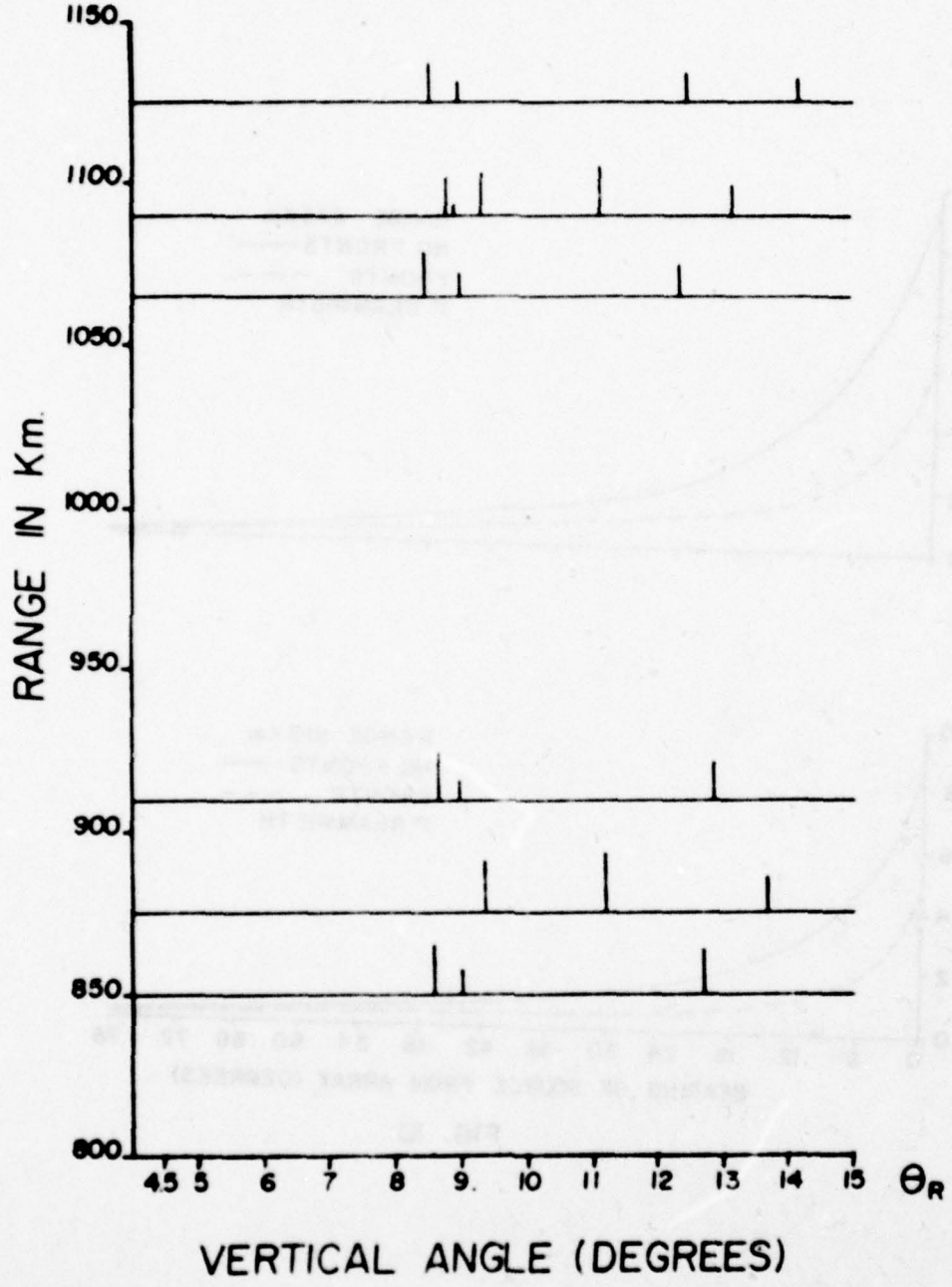
1150
1100
1050
1000
950
900
850
800
RANGE IN Km.
4.5 5 6 7 8 9. 10 11 12 13 14 15 θ_R
VERTICAL ANGLE (DEGREES)

FIG. 11

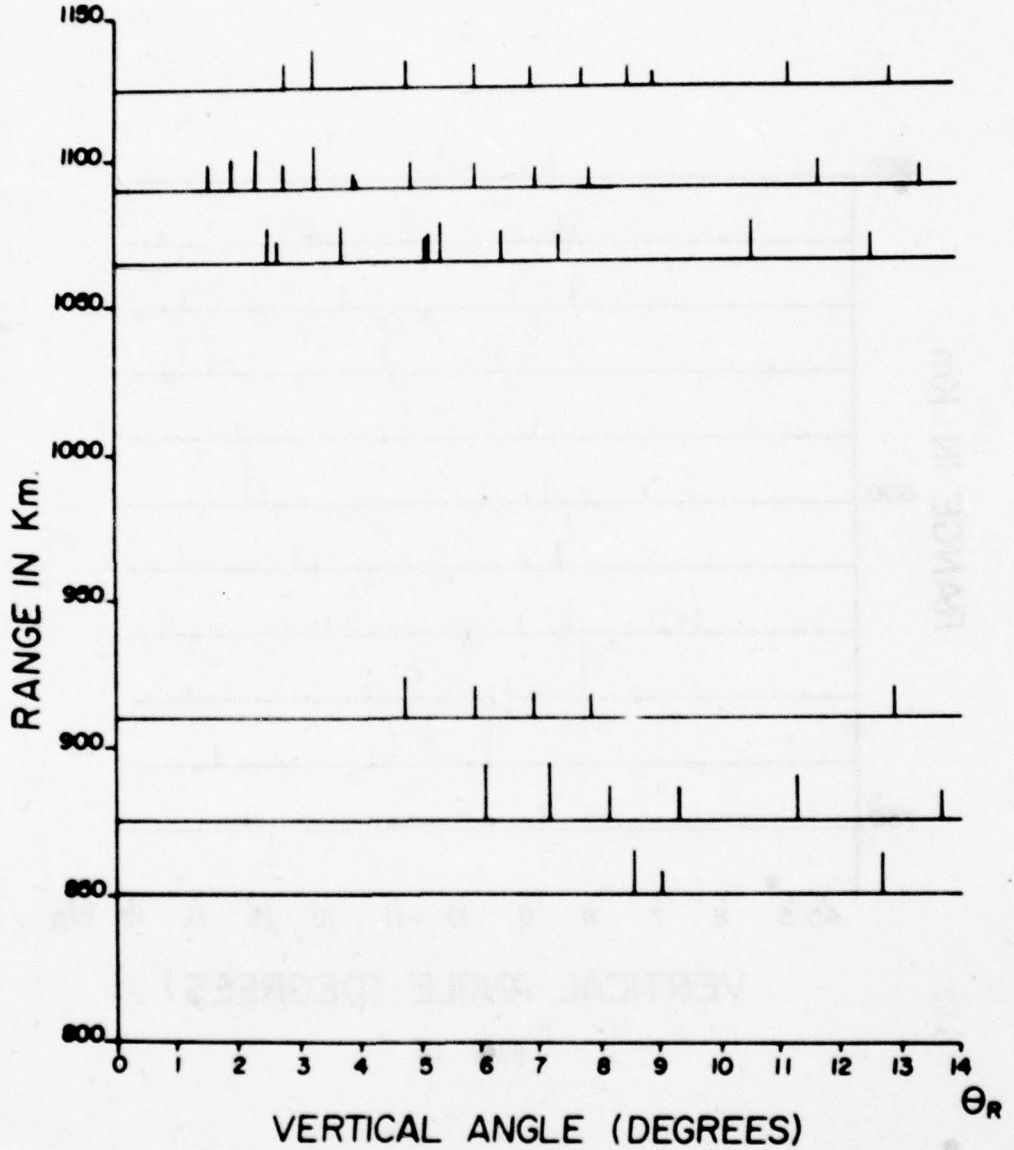
1150
1100
1050
1000
950
900
850
800
RANGE IN Km.
0 1 2 3 4 5 6 7 8 9 10 11 12 13 14
Θ_R
VERTICAL ANGLE (DEGREES)

FIG. 12

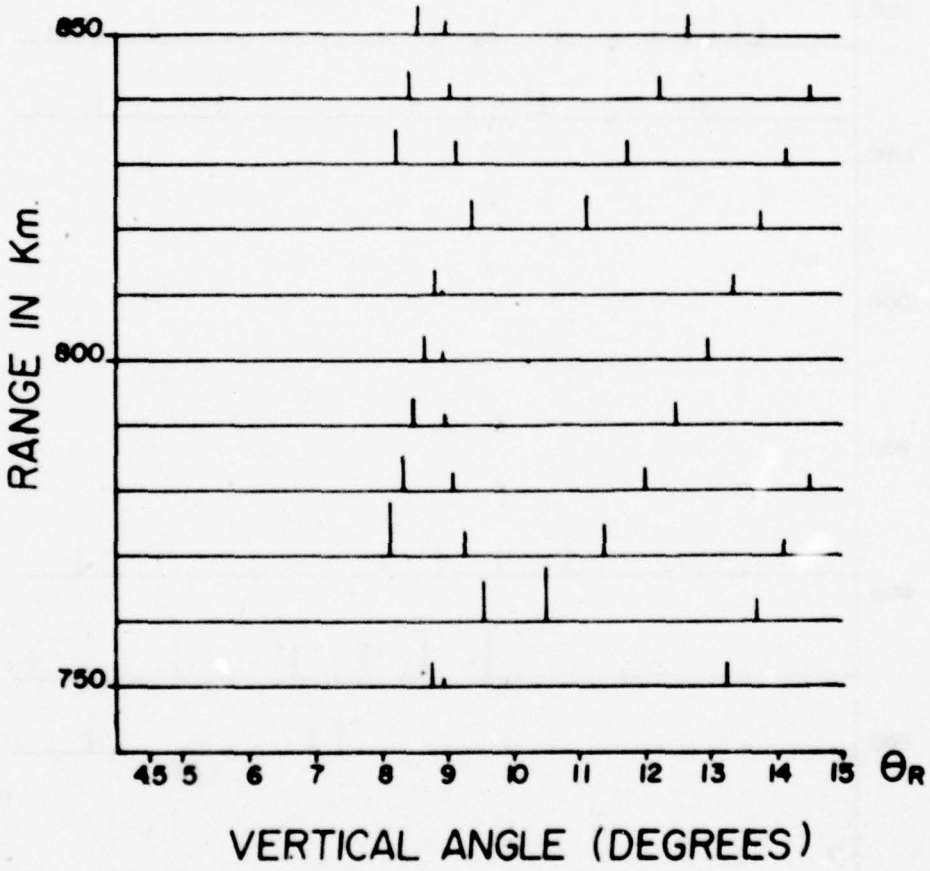
850
800
750
RANGE IN Km
4.5 5 6 7 8 9 10 11 12 13 14 15 θR
VERTICAL ANGLE (DEGREES)

FIG. 13

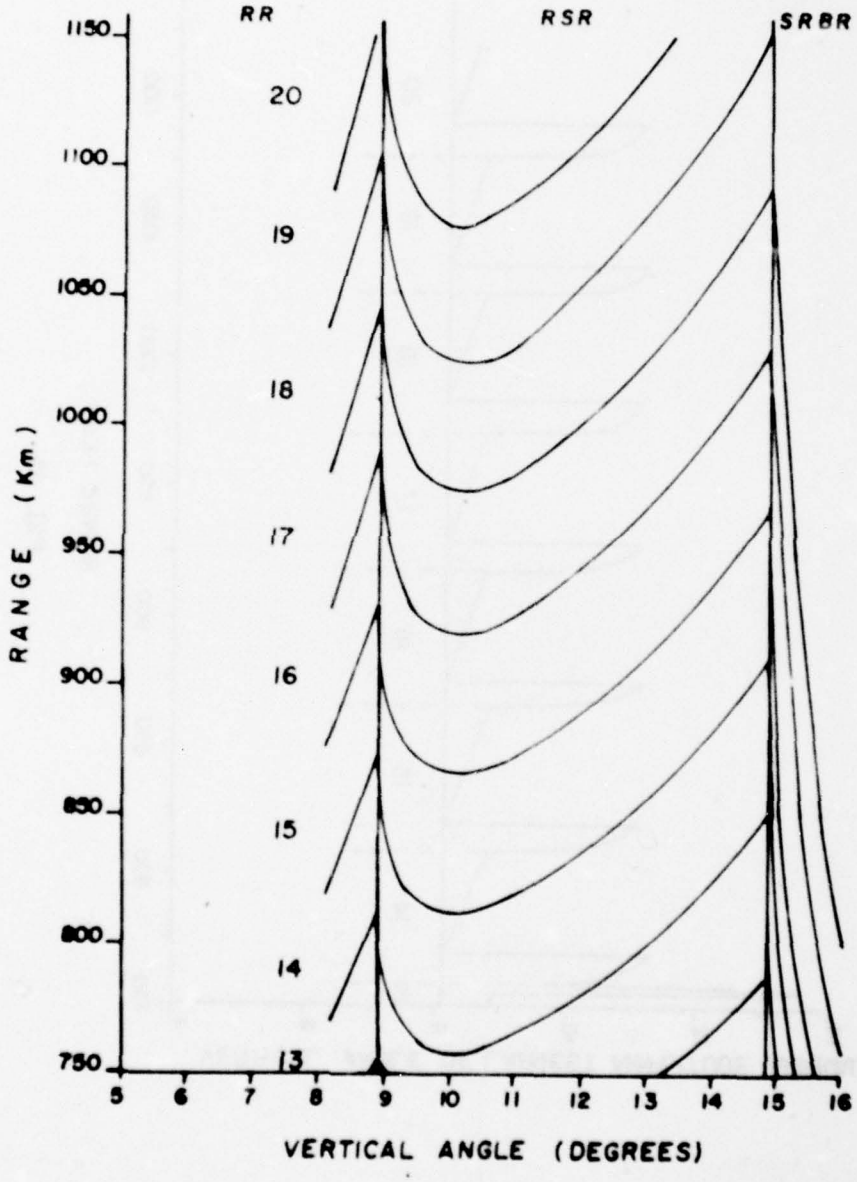
RR
RSR
SRBR
20
19
18
17
16
15
14
13
1150
1100
1050
1000
950
900
850
800
750
RANGE (Km)
5
6
7
8
9
10
11
12
13
14
15
16
VERTICAL ANGLE (DEGREES)

FIG. 14

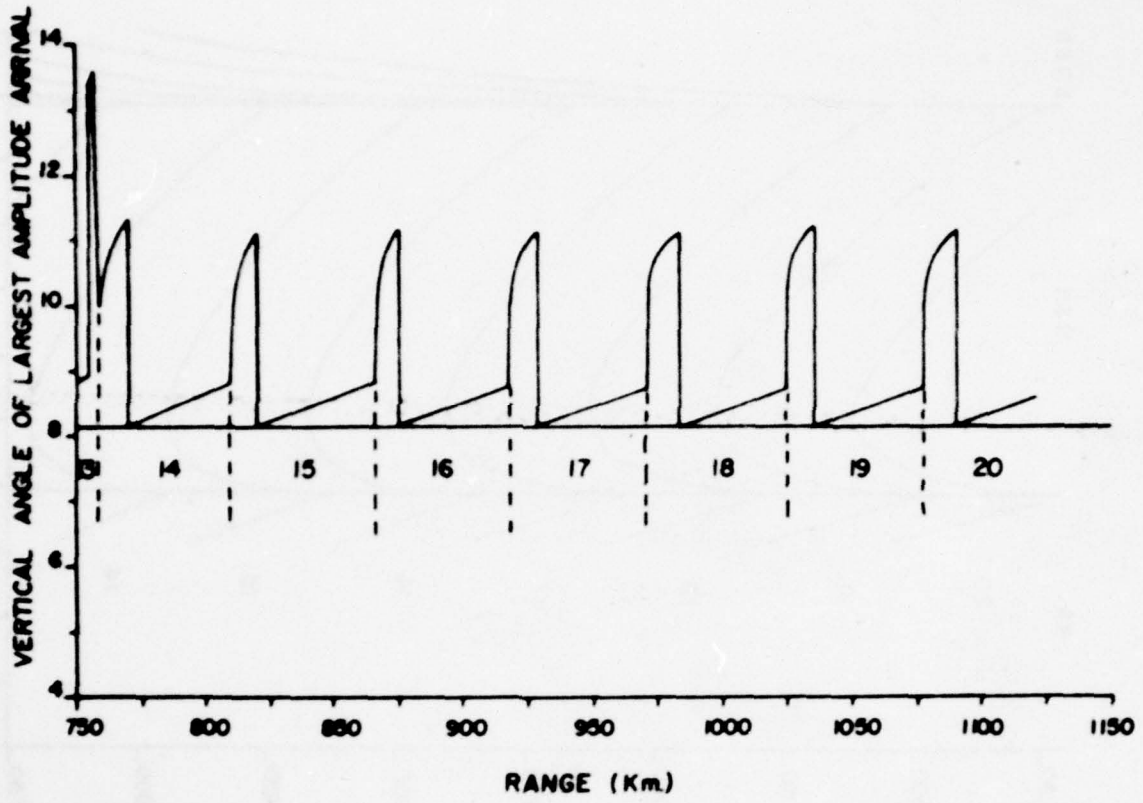
VERTICAL ANGLE OF LARGEST AMPLITUDE ARRIVAL
14
12
10
8
6
4
13
14
15
16
17
18
19
20
750
800
850
900
950
1000
1050
1100
1150
RANGE (Km)

FIG. 15

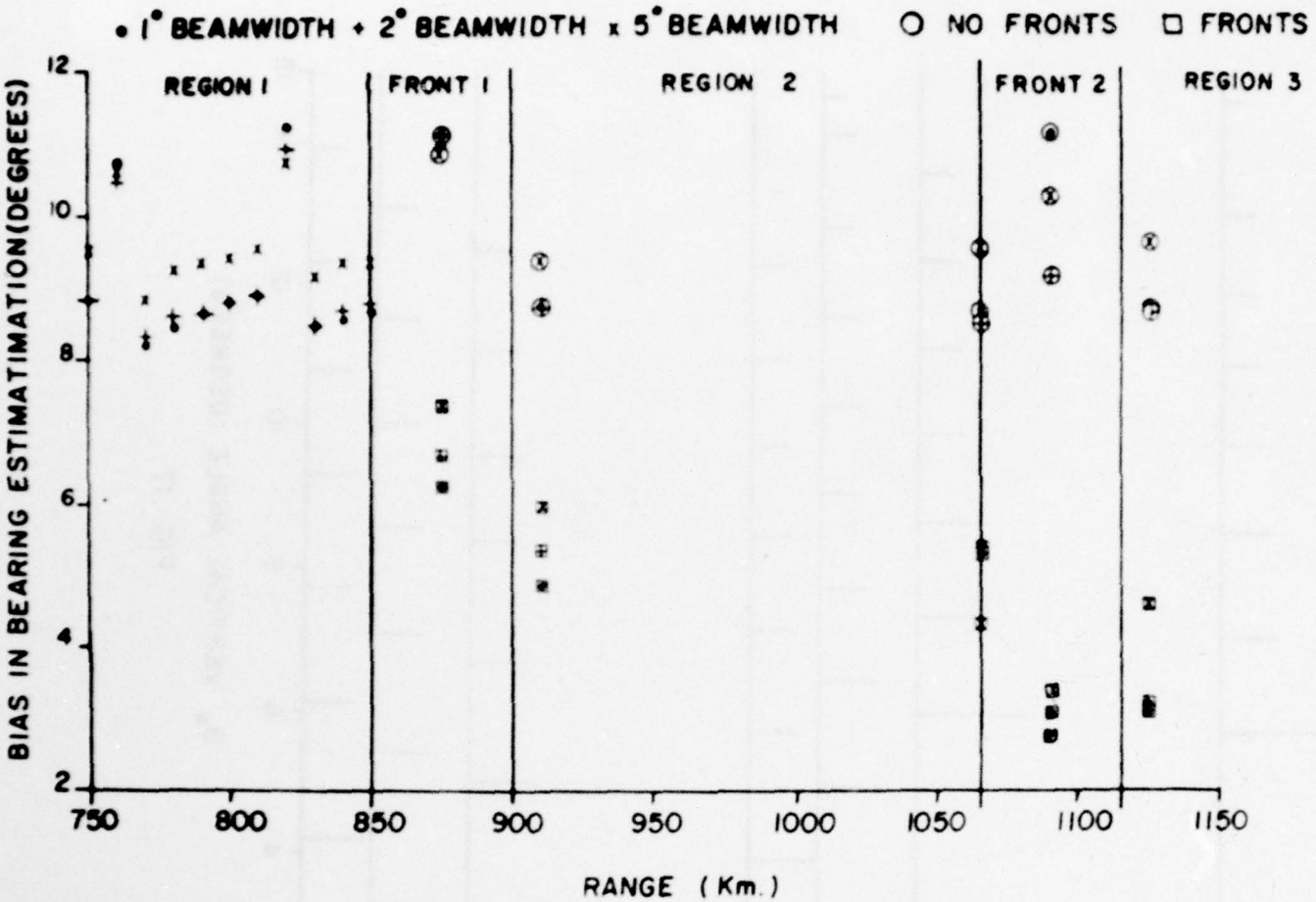

BIAS IN BEARING ESTIMATION AT ENDFIRE

FIG. 16

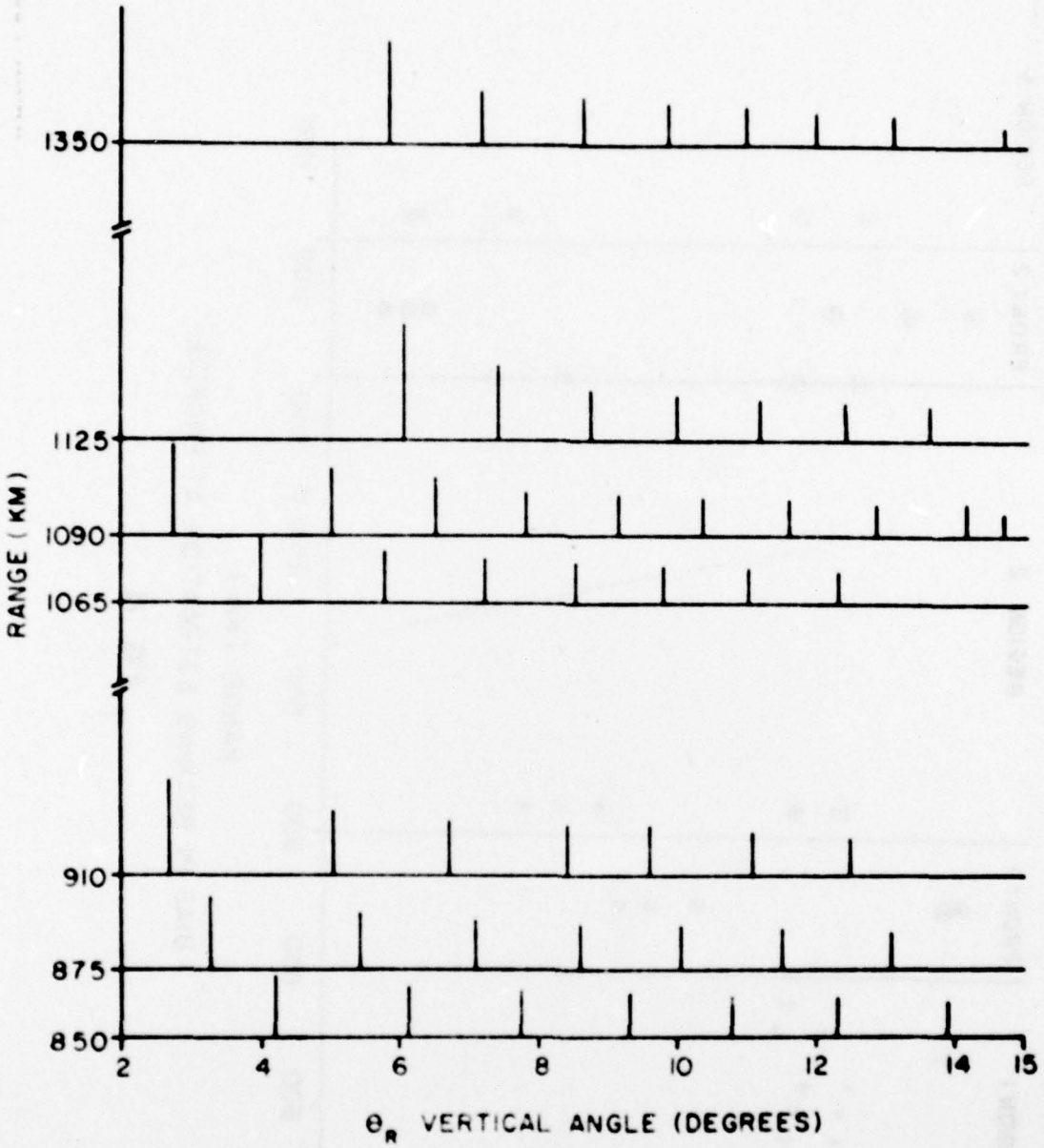
1350
1125
1090
1065
910
875
850
RANGE (KM)
2
4
6
8
10
12
14
15
θ_R VERTICAL ANGLE (DEGREES)

FIG. 17

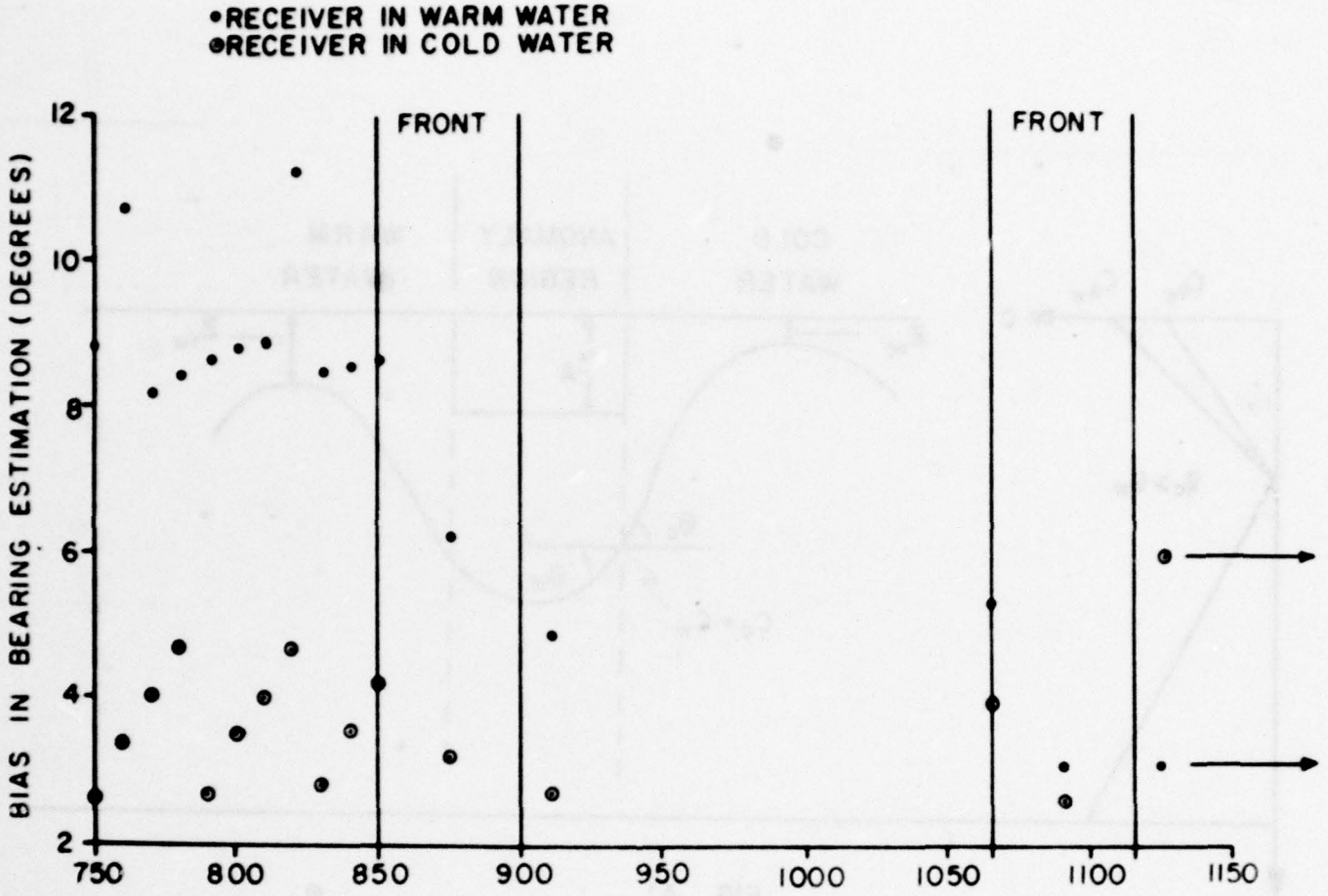

BIAS IN BEARING ESTIMATION AT ENDFIRE

FIG. 18

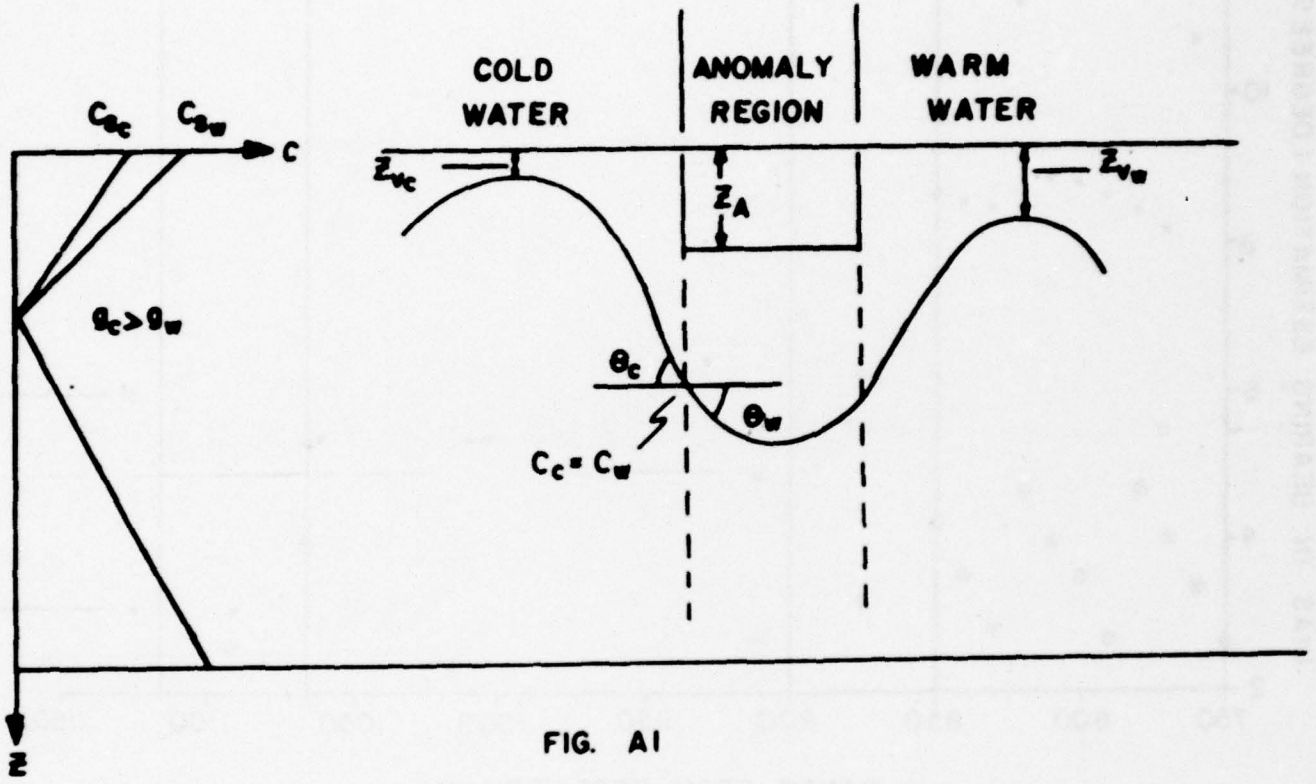
COLD
WATER
ANOMALY
REGION
WARM
WATER
C_{sc}
C_{sw}
C
Z_{wc}
Z_A
Z_{ww}
$\theta_c > \theta_w$
θ_c
θ_w
$C_c = C_w$
Z

FIG. A1

UNCLASSIFIED DISTRIBUTION LIST

	Copies
Office of Naval Research 800 North Quincy Street Arlington, Virginia 22217 Attn: Code 222	2
102B	1
480	1
486	1
210	1
220	1
Director Naval Research Laboratory 4555 Overlook Avenue, S.W. Washington, D.C. 20375 Attn: Dr. J.P. Dugan	1
Dr. D.R. Palmer	1
Dr. J.C. Munson	1
Mr. R.R. Rojas	1
Dr. B.B. Adams	1
Dr. W.B. Moseley	1
Unclassified Library	1
Superintendent Naval Research Laboratory Underwater Sound Reference Division P.O. Box 8337 Orlando, Florida 32806	1
Director Office of Naval Research Branch Office 1030 East Green Street Pasadena, California 91106	1
Office of Naval Research Rm 239, Campbell Hall University of California Berkeley, Calif. 94720	1
Director Office of Naval Research Branch Office 495 Summer Street Boston, Massachusetts 02210	1
Office of Naval Research New York Area Office 715 Broadway - 5th Floor New York, New York 10003	1
Commanding Officer Office of Naval Research Branch Office Box 39 FPO New York 09510	1

UNCLASSIFIED DISTRIBUTION LIST

Director Office of Naval Research Branch Office 536 South Clark Street Chicago, Illinois 60605	1
Office of Naval Research Resident Representative University District Building, Rm 422 1107 N.E. 45th Street Seattle, Washington 98105	1
Office of Naval Research Resident Representative Lamont-Doherty Geological Observatory Palisades, New York 10964	1
Technical Director Naval Oceanographic R&D Agency NSTL Station Bay St. Louis, Mississippi 39522	
Att: Dr. Ralph Goodman	1
Mr. E. Smith	1
CDR J.E. Paquin	1
Mr. K.W. Lackie	1
Mr. R. Van Wyckhouse	1
Dr. S.W. Marshall	1
Mr. G. Lewis	1
Director Naval Oceanographic Office NSTL Station Bay St. Louis, Mississippi 39522	
Attn: Dr. B.E. Olson	1
Dr. T.M. Davis	1
Mr. W.H. Geddes	1
Mr. M.K. Schank	1
Mr. R.A. Peloquin	1
Mr. R. Merrifield	1
Dr. W. Jobst	1
Office of the Assistant Secretary of the Navy for Research, Engineering and Systems Rm 4E732, Pentagon Washington, D.C. 20350	1
Chief of Naval Operations Rm. 4E482, Pentagon Washington, D.C. 20350 Attn: Naval Oceanography Division (OP952)	1
Chief of Naval Operations Rm. 5D616, Pentagon Washington, D.C. 20350 Attn: Mr. R. Winokur, OP095E	1

UNCLASSIFIED DISTRIBUTION LIST

Chief of Naval Operations 1
Rm 5D580, Pentagon
Washington, D.C. 20350
Attn: OP951F

Chief of Naval Operations 1
Rm. 4D518, Pentagon
Washington, D.C. 20350
Attn: Capt. J.M. Van Metre

Chief of Naval Operations 1
Office of the Director
Naval Oceanographic Division
OP-952
Department of the Navy
Washington, D.C. 20352
Attn: Dr. R.W. James

Commander 1
Oceanographic System, Atlantic
Box 100
Norfolk, Virginia 23511

Commander 1
Oceanographic System, Pacific
Box 1390
Pearl Harbor, Hawaii 96860

Defense Advanced Research Projects Agency 1
1400 Wilson Blvd.
Arlington, Virginia 22209
Attn: Dr. R. Gustafson

ARPA Research Center 1
Moffett Field Unit #1
California 94035
Attn: Mr. E. Smith

Commanding Officer 1
Fleet Weather Central
Box 113
Pearl Harbor, Hawaii 96860
Attn: CDR C. Dunlop

Naval Ocean Systems Center (Kaneohe) 2
Kaneohe, Hawaii 96863
Attn: Mr. D. Hightower
Mr. B. Kishimoto

Commander 2
Naval Electronic Systems Command
2511 Jefferson Davis Highway
National Center #1
Arlington, Virginia 20360
Attn: Capt H. Cox, PME 124
CDR D. Griffith, NAVELEX 320

UNCLASSIFIED DISTRIBUTION LIST

Commander 1
Naval Air Systems Command
Jefferson Plaza #1
1411 Jefferson Davis Highway
Arlington, Virginia 20360

Commander
Naval Sea Systems Command
National Center #2
2521 Jefferson Davis Highway
Arlington, Virginia 20362
Attn: SEA 037 1
Mr. Carey Smith, 06H1 1
CDR David F. Bolka, 06H2 1
SEA 003 1

Commanding Officer
Fleet Numerical Weather Central
Monterey, California 93940
Attn: Mr. Paul Stevens 1
Dr. D.R. McLain (NMFS) 1

Defense Documentation Center 12
Cameron Station
Alexandria, Virginia 22314

Director of Navy Laboratories 2
Chief of Naval Material
2211 Jefferson Davis Highway
Crystal Plaza #5
Arlington, Virginia 20360
Attn: Dr. James Probus, NAVMAT 08T1
Dr. Tibor Horwath, NAVMAT 08T2

Commander 4
Naval Ocean Systems Center
Department of the Navy
San Diego, Calif. 92132
Attn: Dr. Daniel Andrews
Dr. Dean Hanna
Mr. Henry Aurand
Dr. Harry A. Schenck

Commander 1
Naval Surface Weapons Center
Acoustics Division
Silver Spring, Maryland 20910
Attn: Dr. Zaka Slawsky

Commander 1
Naval Surface Weapons Center
Science and Mathematics Research Group (K05)
Dahlgren, Virginia 22448
Attn: Dr. E.W. Schwiderski

UNCLASSIFIED DISTRIBUTION LIST

Commanding Officer 6
Naval Underwater Systems Center
New London Laboratory
New London, Connecticut 06320
Attn: Dr. W. Von Winkle
Dr. A. Nuttall
Mr. A. Ellinthorpe
Dr. D.M. Viccione
Mr. A. Donn Cobb
Mr. R. Hasse

Commander 1
Naval Air Development Center
Department of the Navy
Warminster, Pennsylvania 18974
Attn: Keith Jerome, Proj. Eng.

Commanding Officer 1
Naval Coastal Systems Laboratory
Panama City, Florida 32401
Attn: Unclassified Library

Commanding Officer 1
Naval Underwater Systems Center
Newport Laboratory
Newport, Rhode Island 02840
Attn: Unclassified Library

Commander 1
Naval Ship R&D Center
Bethesda, Maryland 20034
Attn: Dr. M. Sevik

Commander 1
David W. Taylor Naval Ship R&D Center
Bethesda, Maryland 20084

Superintendent 1
Naval Postgraduate School
Monterey, California 93940

Superintendent 1
U.S. Naval Academy
Annapolis, Maryland 21402
Attn: Library

Commanding Officer 3
Naval Intelligence Support Center
4301 Suitland Road
Washington, D.C. 20390
Attn: Dr. Johann Martinek
Mr. E. Bissett
NISC 34

UNCLASSIFIED DISTRIBUTION LIST

Director 2
Applied Physics Laboratory
University of Washington
1013 N.E. 40th Street
Seattle, Washington 98105
Attn: Dr. T.E. Ewart
Dr. M. Schulkin

Applied Research Laboratories 2
University of Texas at Austin
P.O. Box 8029
10000 FM Road 1325
Austin, Texas 78712
Attn: Dr. Loyd Hampton
Dr. Charles Wood

Institute of Geophysics and 3
Planetary Physics
Scripps Institute of Oceanography
University of California
La Jolla, California 92093
Attn: Dr. W. Munk
Mr. J. Spiesberger
Dr. V.C. Anderson

Dr. Melvin J. Jacobson 1
Rensselaer Polytechnic Institute
Troy, New York 12181

Dr. T.G. Birdsall 1
Cooley Electronics Laboratory
University of Michigan
Ann Arbor, Michigan 48105

Dr. M.A. Basin 1
S.D.P. Inc
15250 Ventura Blvd.
Suite 518
Sherman Oaks, Calif. 91403

University of Miami 2
Rosenstiel School of Marine and
Atmospheric Sciences
4600 Rickenbacker Causeway
Miami, Florida 33149
Attn: Dr. H. DeFerrari
Dr. W. Duing

Dr. David Middleton 1
127 East 91st Street
New York, New York 10028

UNCLASSIFIED DISTRIBUTION LIST

Dr. Donald Tufts 1
University of Rhode Island
Department of Electrical Eng.
Wakefield, Rhode Island 02881

Dr. Loren Nolte 1
Duke University
Department of Electrical Engineering
Durham, North Caroline 27706

Mr. S.W. Autrey 1
Hughes Aircraft Company
P.O. Box 3310
Fullerton, Calif. 92634

Dr. Thomas W. Ellis 1
Texas Instruments, Inc.
13500 N. Central Expressway
Dallas, Texas 75231

Mr. Carl Hartdegen 1
Palisades Sofar Station
Bermuda Division of Palisades
Geophysical Institute
FPO New York 09560

Mr. Beaumont Buck 1
Polar Research Laboratory
123 Santa Barbara Avenue
Santa Barbara, Calif. 93101

Dr. M. Weinstein 1
Underwater Systems, Inc.
8121 Georgia Avenue
Silver Spring, Maryland 20910

Dr. Thomas G. Kincaid 1
General Electric Company
P.O. Box 1088
Schenectady, New York 12301

Dr. C.N.K. Mooers 1
University of Delaware
Newark, Delaware 19711

Woods Hole Oceanographic Institute 2
Woods Hole, Massachusetts 02543
Attn: Dr. Paul McElroy
Dr. R. Spindel

UNCLASSIFIED DISTRIBUTION LIST

Dr. Richard James c/o Fleet Weather Facility 4301 Suitland Road Washington, D.C. 20390	1
Atlantic Oceanographic and Meteorological Laboratories 15 Rickenbacker Causeway Miami, Fla. 33149 Attn: Dr. John Proni	1
Research Triangle Institute Research Triangle Park Durham, North Carolina 27709 Attn: Dr. E.G. Baxa, Jr.	1
Science Applications, Inc. 8400 Westpartk Drive McLean, Virginia 22102 Attn: Ms. Angela D'Amico Ms. Lorna Blumen	2
Bell Telephone Laboratories 1 Whippany Road Whippany, New Jersey 07981 Attn: Dr. Bruce Bogart Dr. Peter Hirsch	2
General Electric Company Heavy Military Electronic Systems Syracuse, New York 13201 Attn: Mr. Don Winfield	1
Javcor Incorporated 205 S. Whiting Street Suite 607 Alexandria, Virginia 22304 Attn: Dr. S. Adams	1

UNCLASSIFIED

SECURITY CLASSIFICATION OF THIS PAGE (When Data Entered)

REPORT DOCUMENTATION PAGE	READ INSTRUCTIONS BEFORE COMPLETING FORM
1. REPORT NUMBER: 79002	2. GOVT ACCESSION NO. / 3. RECIPIENT'S CATALOG NUMBER
4. TITLE (and Subtitle): Effects of Ocean Fronts on Multipath Vertical Angles and the Associated Biases in Array Bearing Estimation	5. TYPE OF REPORT & PERIOD COVERED / 6. PERFORMING ORG. REPORT NUMBER
7. AUTHOR(s): R.P. Flanagan and X. Zabalgogeazcoa	8. CONTRACT OR GRANT NUMBER(s): N00014-74-C-0229
9. PERFORMING ORGANIZATION NAME AND ADDRESS: Institute for Acoustical Research, 615 S.W. 2nd Avenue, Miami, Fla. 33130	10. PROGRAM ELEMENT, PROJECT, TASK AREA & WORK UNIT NUMBERS
11. CONTROLLING OFFICE NAME AND ADDRESS: Procuring Contracting Officer, Office of Naval Research, Dept. of the Navy, Arlington, Va. 22217	12. REPORT DATE: July 1979 / 13. NUMBER OF PAGES: 45
14. MONITORING AGENCY NAME & ADDRESS(if different from Controlling Office): Office of Naval Research Resident Rep. Columbia University Lamont Doherty Geological Observatory Torrey Cliff, Palisades, New York 10913	15. SECURITY CLASS. (of this report): Unclassified / 15a. DECLASSIFICATION/DOWNGRADING SCHEDULE

16. DISTRIBUTION STATEMENT (of this Report)

Distribution of this Document is unlimited

12 55

17. DISTRIBUTION STATEMENT (of the abstract entered in Block 20, if different from Report)

18. SUPPLEMENTARY NOTES

19. KEY WORDS (Continue on reverse side if necessary and identify by block number)

ocean fronts
propagation
bearing estimation
ray model

20. ABSTRACT (Continue on reverse side if necessary and identify by block number)

An oceanic frontal system perpendicular to the propagation path is modeled with a deep receiver in warm water and a shallow source which is moved through the frontal system into progressively colder water. A ray model is used to calculate the arrival structure and determine the effects of the frontal system on ray amplitude and vertical angle. The receiving horizontal line array determines the bias in bearing estimation resulting from →

DD FORM 1 JAN 73 1473 EDITION OF 1 NOV 65 IS OBSOLETE S/N 0102-014-6601

408 141

UNCLASSIFIED

SECURITY CLASSIFICATION OF THIS PAGE (When Data Entered)

the changing multipath structure. This bias is found to be heavily dependent on array orientation and range into the frontal system while being only slightly dependent on array beamwidth. The underlying physics causing the multipath variations is the frontal system acting as a focusing lens. When the transducer positions are reversed, that is a deep receiver in cold water and a shallow source in progressively warmer water, the frontal system acts as a diverging lens.